

Electron spin relaxation in carbon nanotubes

Y. G. Semenov, J. M. Zavada, and K. W. Kim

*Department of Electrical and Computer Engineering,
North Carolina State University, Raleigh, NC 27695-7911*

Abstract

The long standing problem of inexplicably short spin relaxation in carbon nanotubes (CNTs) is examined. The curvature-mediated spin-orbital interaction is shown to induce fluctuating electron spin precession causing efficient relaxation in a manner analogous to the Dyakonov-Perel mechanism. Our calculation estimates longitudinal (spin-flip) and transversal (decoherence) relaxation times as short as 150 ps and 110 ps at room temperature, respectively, along with a pronounced anisotropic dependence. Interference of electrons originating from different valleys can lead to even faster dephasing. The results can help clarify the measured data, resolving discrepancies in the literature.

PACS numbers: 85.35.Kt, 85.75.-d, 81.07.Vb, 75.76.+j

Spin-related effects in carbon nanotubes (CNTs) have attracted much attention in recent years [1]. Initially, it was assumed that a weak spin-orbital interaction (SOI) in CNTs, due to p_z -electrons, would lead to a long spin relaxation (and spin coherence length) compared with typical semiconductors. However, numerous experimental measurements of spin transport and electron spin resonance in CNTs present very disparate results for the magnitude of the spin relaxation time τ_s . The processing possibilities for spin transport impose spin conservation at least for the dwell time τ_d of the electrons in CNT [2] providing a lower limit for τ_s . Such approach, however, does not guarantee the direct derivation of τ_s , moreover, association of τ_d with time of electron drift between ferromagnetic contacts leads to enormous discrepancy with spin relaxation time measured by other methods. For example, a drift time around a ps attributes to magnetoresistance (MR) measurements in Refs. 3 and 4, while the electron spin resonance indicates much longer $\tau_s \approx 5$ ns at temperature $T = 300$ K [5]. Sufficient progress in the analysis of spin transport in CNT has been provided in Ref. 6 where both $\tau_d = 60$ ns and $\tau_s = 30$ ns were extracted from MR measurements at $T \leq 120$ K.

A theoretical approach to spin relaxation based on hyperfine interaction [7] failed to explain the short spin relaxation in CNT, even through a recent study [8] corrected the hyperfine interaction constant by two orders of magnitude, still making the spin relaxation longer than $100 \mu\text{s}$. While the carbon intra-atomic SOI has been evaluated as 12 meV [9], higher orders of perturbation theory result in extremely weak spin-orbital coupling ($\sim 1 \mu\text{eV}$) for planar graphene [10]. Thus there is a negligible effect on spin relaxation in CNTs.

Recently such an assumption was revised theoretically [10–14] and experimentally [15] because graphene curvature in CNTs produces mixing of π and σ electron states that can drastically enhance SOI. Qualitatively, it can be viewed as electron spin in a magnetic field stemmed from a clockwise or counterclockwise circular motion around the CNT's circumference. States with opposite electron motion originate from the two different valleys K and K' [11]. The finding of so strong SOI was shown to be responsible for an efficient mechanism of electron spin-lattice relaxation in CNT quantum dots at low temperatures [16]. The actual mechanism of itinerate electron spin relaxation in CNTs at room temperature still presents a very intriguing problem for carbon based spintronics.

We begin with a few essential definitions concerning CNTs [17]. The CNT is conveniently imagined as a spiral graphite sheet (graphene) rolled along the chiral vector \mathbf{C}_h (see Fig. 1).

Here $\mathbf{C}_h = n_a \mathbf{a} + n_b \mathbf{b}$, where $\mathbf{a} = a(1, 0)$ and $\mathbf{b} = a(1/2, \sqrt{3}/2)$ are the graphene lattice unit vectors with $a = 0.246$ nm and n_a and n_b are integers, which characterize the geometry of a particular CNT. The slope of \mathbf{C}_h is defined by $\tan \theta = \sqrt{3}n_b/(2n_a + n_b)$ and the diameter of the CNT is given by $d = |\mathbf{C}_h|/\pi$. The energy band structure of graphene possesses two non-equivalent valleys with Dirac-like dispersion law in the vicinity of Fermi level [18]. They are located at the $K = \frac{2\pi}{3a}(1, \sqrt{3})$ and $K' = \frac{2\pi}{3a}(-1, \sqrt{3})$ corner points of the first Brillouin zone, which will be labeled by $\lambda = 1, -1$ respectively.

The graphene two-valley band structure projects onto the CNT one so that in the vicinity of each valley the kP Hamiltonian takes the form $H_\lambda = \hbar v_F(\lambda \kappa_m \hat{\sigma}_1 + k \hat{\sigma}_2)$ [17] where the Fermi velocity is $v_F = 8 \cdot 10^7$ cm/s and Pauli matrixes $\hat{\sigma}_1$ and $\hat{\sigma}_2$ are defined over the sublattice electronic states A and B. The wave vector \mathbf{k} with respect to K ($\lambda = 1$) or K' ($\lambda = -1$) point is directed along the principal axis ζ of CNT. The rolling along the perpendicular direction ρ (Fig. 1) imposes a quantization of the electron momentum in circumcircular direction fixing the wave numbers $\kappa_m = 2(m - \lambda\nu/3)/d$ with integer magnetic quantum number m and ν (from the set 1, 0, -1) so that $2n_a + n_b + \nu$ becomes divisible by 3. If the CNT is subjected to a magnetic field \mathbf{B}_0 the Aharonov-Bohm magnetic flux passing through the CNT cross section $\phi_{AB} = B_0 \cos \alpha \pi d^2/4$ modifies the quantization condition [17],

$$\kappa_{m,\lambda} = 2(m - \lambda\nu/3 + \phi_{AB}/\phi_0)/d, \quad (1)$$

where α is an angle between \mathbf{B}_0 and CNT axis, $\phi_0 = 2\pi\hbar c/|q_0|$ is the flux quantum, q_0 the electron charge.

The eigenvalues of Hamiltonian H_λ describe the CNT electronic spectrum without spin structure,

$$\varepsilon_{k,m,\lambda} = \pm \hbar v_F \sqrt{\kappa_{m,\lambda}^2 + k^2}, \quad (2)$$

where $+$ ($-$) corresponds to the conduction (valence) band. The CNTs with $\nu = \pm 1$ possess the semiconducting spectrum, with bandgap $E_g = 4\hbar v_F/3d$ even at zero magnetic field, with potential applications in spintronics [1]. We assume $\nu = 1$ in further numerical calculations.

When a spin-orbital interaction is incorporated in the Hamiltonian H_λ , the SOI mediated by CNT curvature which takes the simplest form in CNT co-ordinates ξ, η, ζ (Fig. 1) as:

$$H_{SO} = \Delta_0 \lambda \hat{\sigma}_0 2S_\zeta + \Delta_1 \lambda \hat{\sigma}_1 2S_\zeta - i\Delta_2 \hat{\sigma}_2 (S_+ e^{i\varphi} - S_- e^{-i\varphi}), \quad (3)$$

where $\hat{\sigma}_0$ is 2×2 identical matrix, $S_{\pm} = S_{\xi} \pm iS_{\eta}$, $\varphi = 2\rho/d$, $0 < \rho < |\mathbf{C}_h|$. In (3) the spin-orbital constants are proportional to CNT curvature, $\Delta_0 = (\delta_0/d) \cos 3\theta$, $\Delta_{1,2} = \delta_{1,2}/d$ where the parameter $\delta_1 = -0.19 \text{ meV}\cdot\text{nm}$ has been measured [19] and the ratios $\delta_0/\delta_1 = 4.5$ and $\delta_2/\delta_1 = -1.4$ can be estimated theoretically [10–12]. The Δ_0 depends on CNT chirality so that Δ_0 is maximum in zigzag CNTs ($\theta = 0$) and minimum ($\Delta_0 = 0$) in armchair ones ($\theta = \pi/6$) [12].

These estimates show that the SOI may be treated as a perturbation for actual electronic energies, i.e., $|\Delta_i| \ll |\varepsilon_{k,m,\lambda}|$. In the first order, the quantum averaging of the H_{SO} on the eigenvectors $|k, m, \lambda\rangle$ of Hamiltonian H_{λ} gives rise to the reduced Hamiltonian of SOI H'_{SO} of electron spin energy in an effective field \mathbf{B}'_{SO} directed along the principal axis ζ of the CNT, $H'_{SO} = g\mu_B B'_{SO} S_{\zeta}$, where $g\mu_B B'_{SO} = 2\lambda(\Delta_0 + \Delta_1 \sigma_1)$. We take into account that $\langle k, m, \lambda | \hat{\sigma}_0 | k, m, \lambda \rangle = 1$, $\langle k, m, \lambda | \hat{\sigma}_2 e^{\pm i\varphi} | k, m, \lambda \rangle = 0$ and

$$\sigma_1 = \langle k, m, \lambda | \hat{\sigma}_1 | k, m, \lambda \rangle = \mp \frac{\lambda \varkappa_{m,\lambda}}{\sqrt{k^2 + \varkappa_m^2}}. \quad (4)$$

Here \mp in Eq. (4) corresponds to conduction (valence) band.

An important issue of Eq. (4) is the dependence of $\mathbf{B}'_{SO}(\sigma_1)$ on k i.e. electronic energy [eq. (2)]. This effect can be understood as a result of diminishing of electron velocity v_{\perp} in the ρ -direction with increasing k_{\parallel} along the CNT axis under constant total electron velocity v_F , i.e. $v_{\perp}/v_F = k_{\perp}/|\mathbf{k}| = k_{\perp}/\sqrt{k_{\perp}^2 + k_{\parallel}^2}$ that appears as a factor in Eq. (4) at $k_{\parallel} = k$ and $k_{\perp} = \varkappa_{m,\lambda}$.

It is convenient to introduce the mean values $\langle \sigma_1 \rangle = \sum_m \int \sigma_1 f(\varepsilon_{k,m,\lambda}) dk / \sum_m \int f(\varepsilon_{k,m,\lambda}) dk$ and $B_{SO} = \langle B'_{SO} \rangle = 2\lambda(\Delta_0 + \Delta_1 \langle \sigma_1 \rangle) / g\mu_B$, where $f(\varepsilon_{k,m,\lambda})$ is a thermal population factor for electron with energy $\varepsilon_{k,m,\lambda}$. Correspondingly, the SOI can be separated into a steady part $g\mu_B B_{SO} S_{\zeta}$ and a fluctuating one ΩS_{ζ} with

$$\Omega = 2\Delta_1 \lambda (\sigma_1 - \langle \sigma_1 \rangle). \quad (5)$$

Fluctuations in k lead to fluctuations of the effective spin-orbital field and serve as a mechanism of spin relaxation in CNTs. Our analysis centers on the efficiency of this mechanism for CNTs in the presence of an external magnetic field \mathbf{B}_0 . This supplements the Hamiltonian H_{SO} with a Zeeman interaction $H_Z = g\mu_B \mathbf{B}_0 \mathbf{S}$. The joint action determines a spin energy $g\mu_B \mathbf{B}_{eff} \mathbf{S}$ in an effective field $\mathbf{B}_{eff} = \mathbf{B}_{SO} + \mathbf{B}_0$.

In the reference frame (ξ, η, ζ) , the Zeeman Hamiltonian takes the form $H_Z = \hbar\omega_Z(\sin\alpha S_\xi + \cos\alpha S_\zeta)$, $\hbar\omega_Z = g\mu_B B_0$ ($g = 2$ and μ_B is the Bohr magneton) so that the frequency of spin precession $\omega_\lambda = g\mu_B B_{eff}/\hbar$ in a total effective field \mathbf{B}_{eff} is [20]

$$\omega_\lambda = \sqrt{(\omega_Z \sin\alpha)^2 + [\omega_Z \cos\alpha + 2\lambda(\Delta_0 + \Delta_1 \langle\sigma_1\rangle)/\hbar]^2}. \quad (6)$$

Spin relaxation is conveniently described in other co-ordinates X, Y and Z , where Z is a spin quantization axis defined by the \mathbf{B}_{eff} . Correspondingly, evolution of S_Z and S_X, S_Y correlates with longitudinal (spin-flip) and transversal (phase) spin relaxation. The angle α_λ ($0 \leq \alpha_\lambda \leq \pi$) of \mathbf{B}_{eff} slope to CNT axis defines

$$\cos\alpha_\lambda = [\hbar\omega_Z \cos\alpha + 2\lambda(\Delta_0 + \Delta_1 \langle\sigma_1\rangle)]/\hbar\omega_\lambda. \quad (7)$$

In a second quantization representation, the operator of fluctuating field takes the form $\Omega = \sum_{k,m} \mathbf{b}(k,m)n_{k,m}$, $n_{k,m} = a_{k,m}^\dagger a_{k,m}$, where $a_{k,m}^\dagger$ and $a_{k,m}$ are creation and annihilation operators and the vector $\mathbf{b}(k,m) = 2\Delta_1\lambda(\sigma_1 - \langle\sigma_1\rangle)(-\sin\alpha_\lambda, 0, \cos\alpha_\lambda)$ is expressed in co-ordinates X, Y , and Z .

Assuming a short correlation time τ_p for the electronic correlation function $\langle n_{k,m}(t)n_{k,m} \rangle$ in comparison with the spin relaxation time τ_S , one can use the Markovian equations of spin evolution in form of expanded Bloch equations in which the spin mean values $\langle \mathbf{S} \rangle = Tr\hat{\rho}(t)\mathbf{S}$ ($\hat{\rho}(t)$ is a density matrix [21]). Then the spin polarization deviation from thermal equilibrium becomes $\mathbf{P} = 2(\langle \mathbf{S} \rangle - \langle \mathbf{S} \rangle_\infty)$, where $2\langle \mathbf{S} \rangle_\infty = 2\lim_{t \rightarrow \infty} \langle \mathbf{S} \rangle = (0, 0, -\tan\hbar\omega_\lambda/2k_B T)$. These equations take the simplest form in the X, Y, Z coordinate system:

$$\frac{d\mathbf{P}_\lambda}{dt} = (\hat{\omega}_\lambda - \hat{\Gamma}_\lambda) \mathbf{P}_\lambda, \quad (8)$$

where the 3×3 matrix $\hat{\omega}_\lambda$ represents the cross product of $\vec{\omega}_\lambda = (0, 0, \omega_\lambda)$, $\hat{\omega}_\lambda \mathbf{P}_\lambda = \vec{\omega}_\lambda \times \mathbf{P}_\lambda$. Thus, $\hat{\omega}_\lambda$ includes only two non-zero matrix elements $\omega_{YX} = -\omega_{XY} = \omega_\lambda$, and $\hat{\omega}_\lambda \mathbf{S}_0 = \mathbf{0}$. In this case the matrix of relaxation parameters can be reduced to

$$\hat{\Gamma}_\lambda = \begin{pmatrix} R_{XX}^{(\lambda)} & 0 & R_{XZ}^{(\lambda)} \\ 0 & R_{YY}^{(\lambda)} & 0 \\ R_{XZ}^{(\lambda)} & 0 & R_{ZZ}^{(\lambda)} \end{pmatrix}. \quad (9)$$

The low symmetry of the CNT affected by an arbitrary magnetic field produces multiple spin-relaxation parameters $R_{\mu,\nu}^{(\lambda)}$, $\mu, \nu = X, Y, Z$ [four in the case of Eq. (9)], which cannot

be immediately associated with longitudinal or transversal spin relaxation rates. In the most general form they can be represented in terms of Fourier transformation of correlation functions $\langle \Omega_\mu(t) \Omega_\nu \rangle_\omega$ at frequency $\omega = \omega_\lambda$. For spin precession in a fluctuating field they can be evaluated in an approximation of a momentum relaxation time τ_k [21, 22] that assumes explicit knowledge of the τ_k dependence on k . Instead, we use the average value $\tau_p^{-1} = \langle \tau_k^{-1} \rangle$ to evaluate the spin-relaxation characteristics while the specific dependence of τ_k on k can be taken into account by introducing the numerical factor, which is about $Q_1 \simeq 1.5 \div 3$ [22]. Based on a recent study [23] we assign $\tau_p = 1$ ps and assume $Q_1 = 2$ for further numerical calculations.

Applying these approximations we find

$$\begin{aligned}
R_{XX}^{(\lambda)} &= \cos^2 \alpha_\lambda \frac{(2\Delta_1)^2 \tau_p}{\hbar^2} Q_1 \Delta \sigma_1^2; \\
R_{ZZ}^{(\lambda)} &= \sin^2 \alpha_\lambda \frac{(2\Delta_1)^2 \tau_p}{\hbar^2 (\omega_S^2 \tau_p^2 + 1)} Q_1 \Delta \sigma_1^2; \\
R_{YY}^{(\lambda)} &= R_{XX}^{(\lambda)} + R_{ZZ}^{(\lambda)}; \\
R_{XZ}^{(\lambda)} &= \frac{R_{XX}^{(\lambda)}}{2} \tan \alpha_\lambda + \frac{R_{ZZ}^{(\lambda)}}{2} \cot \alpha_\lambda,
\end{aligned} \tag{10}$$

where $\Delta \sigma_1^2 = \langle \sigma_1^2 \rangle - \langle \sigma_1 \rangle^2$ critically depends on the temperature so that $\Delta \sigma_1 \rightarrow 0$ at $T \rightarrow 0$. Results of calculations of the relaxation rate parameters [Eq. (10)] as a function of temperature, magnetic field strength and direction, and CNT diameter are presented in Fig. 2. It can be noticed that there is not a single $R_{\mu\nu}^{(\lambda)}$, which significantly dominates over all ranges of T , \mathbf{B}_0 , and d . Thus the full set of $R_{\mu\nu}^{(\lambda)}$ is required to describe spin relaxation in CNTs. All $R_{\mu\nu}^{(\lambda)}$ are strongly depended on temperature that controls energy dispersion. Moreover, the relaxation rate decreases with an increase of CNT diameter due to SOI reduction with decreasing curvature. The non-monotonic dependence on the external magnetic field strength and its direction depends upon the interplay between \mathbf{B}_{SO} and \mathbf{B}_0 that leads to suppression of $R_{ZZ}^{(\lambda)}$ and $R_{XZ}^{(\lambda)}$ when $\alpha \rightarrow 0$ or $B_0 \rightarrow 0$.

Examples of numerical solutions to Eqs. (8,9,10) are shown in Fig. 3. In particular, interference of spin polarizations from the two non-equivalent valleys can lead to the oscillation amplitude beating shown in Fig. 3(a) where beats alternate with nodes in 90 ps. When the magnetic field is perpendicular to the CNT axis ($\alpha = 90^\circ$), a fast polarization damping is found for longitudinal ($\tau_s \simeq 150$ ps) and transversal ($\tau_s \simeq 110$ ps) spin polarizations as seen in Fig. 3(b). A greater variation of spin relaxation exists in CNTs with different chirality

placed in an arbitrary directed magnetic field.

The developed theory can be applied to MR measurements which are usually carried out on a CNT with weak contacts to source/drain ferromagnets. Electron undergo multiple reflections from the contacts before exiting. In such a case the output signal depends on both spin relaxation time τ_s and electron dwell time τ_d [6]. The experimental setup also provides for electron injection into the CNT with spin polarization along magnetization \mathbf{M}_S of ferromagnetic source and spin detection with a ferromagnetic drain polarized in either the same direction $\mathbf{M}_D = \mathbf{M}_S$ or the opposite one, $\mathbf{M}'_D = -\mathbf{M}_S$. Spin dependent output from each valley ΔI_λ is proportional to difference $\mathbf{m}\bar{\mathbf{P}}_\lambda - \mathbf{m}'\bar{\mathbf{P}}_\lambda = 2\mathbf{m}\bar{\mathbf{P}}_\lambda$ ($\mathbf{m} = \mathbf{M}_D/|\mathbf{M}_D|$, $\mathbf{m}' = -\mathbf{m}$) where the spin polarization is averaged over τ_d ($\bar{\mathbf{P}}_\lambda = \frac{1}{\tau_d} \int_0^\infty \mathbf{P}_\lambda(t) e^{-t/\tau_d} dt$) provided that τ_d is longer than electron drift from source to drain. $\bar{\mathbf{P}}_\lambda$ can be found from Eq. (8) by multiplication with e^{-t/τ_d} and subsequent integration over t . Assuming that the rate of intervalley transitions is less than $R_d = 1/\tau_d$, the total spin-dependent output can be expressed as $\sum_\lambda \Delta I_\lambda / 2 = F_s R_d$, where

$$F_s = c \mathbf{m} \sum_\lambda (\hat{\Gamma}_\lambda + \hat{\mathbf{I}} R_d - \hat{\omega}_\lambda)^{-1} \mathbf{m}. \quad (11)$$

Here c is a dimensional constant and $\hat{\mathbf{I}}$ is the identity 3×3 matrix. In the case of $\omega_\lambda = 0$, $\hat{\Gamma}_\lambda = \hat{\mathbf{I}}/\tau_s$, Eq. (11) reduces to $F_s = c/(\tau_d^{-1} + \tau_s^{-1})$ which is in agreement with previous calculations [6]. In more general situations, the following relation holds

$$\tau_s = - \lim_{R_d \rightarrow 0} \frac{d \ln F_s}{d R_d}. \quad (12)$$

If $\omega_\lambda \gg R_{\mu\nu}^{(\lambda)} \equiv 1/\tau_{\mu\nu}^{(\lambda)}$, the last equation leads to $\tau_s = \sum_\lambda \tau_{ZZ}^{(\lambda)2} / \sum_\lambda \tau_{ZZ}^{(\lambda)}$. Thus, only longitudinal spin relaxation (i.e. spin-flip) can control the magnetoresistance measurements in a CNT at strong magnetic field. In Fig. 3c the calculated dependence of τ_s on the chiral angle θ of the CNT is displayed. For example, $\tau_s \simeq 220$ ps at $T = 300$ K, for the case of $B_0 = 0.5$ T, $d = 2$ nm, $\mathbf{m} \parallel \mathbf{B}_0$ $\alpha = 90^\circ$ and $\theta = 26^\circ$.

However spin relaxation is suppressed at small values of α . The experimental setup treated in Ref. [6] displays a small deviation of the magnetization direction from the CNT axis, with $\alpha \simeq 10^\circ$. For such a case and with $T = 120$ K, $B_0 = 0.1$ T and $d = 10$ nm Eq. (12) predicts $\tau_s \simeq 69$ ns which approaches the measured $\tau_s = 30$ ns. This results indicates the high efficiency of the spin relaxation mechanism even through small symmetry breaking in the design of realistic devices.

In conclusion, we show that the fluctuations of curvature-induced spin-orbital interaction that are associated with electron random motion in CNTs is responsible for the short spin relaxation. If a magnetic field preserves the uniaxial symmetry of CNT, the spin-flip relaxation is suppressed. However a small asymmetry may lead to visible manifestations of this precession change. These issues may stimulate further experiments to determine the optimal conditions for room temperature CNT spintronic device applications.

This work was supported in part by the US Army Research Office, NSF, and the FCRP Center on Functional Engineered Nano Architectonics (FENA).

-
- [1] A. Cottet *et al.*, Semicond. Sci. Technol. **21**, S78 (2006).
 - [2] A. Fert *et al.*, IEEE Trans. Electron Dev. **54**, 921 (2007).
 - [3] K. Tsukagoshi, W. B. Alphenaar, and H. Ago, Nature **401**, 572 (1999).
 - [4] S. Sahoo *et al.*, Nature Phys. **1**, 99 (2005).
 - [5] P. Petit *et al.*, Phys. Rev. B **56**, 9275 (1997).
 - [6] L. E. Hueso *et al.*, Nature **445**, 410 (2007).
 - [7] Y. G. Semenov, K. W. Kim, and G. J. Iafrate, Phys. Rev. B **75**, 045429 (2007).
 - [8] H. O. H. Churchill *et al.*, Nature Phys. **5**, 321 (2009).
 - [9] J. Serrano, M. Cardona, and J. Ruff, Solid State Commun. **113**, 411 (2000).
 - [10] D. Huertas-Hernando, F. Guennea, and A. Brataas, Phys. Rev. B **74**, 155426 (2006).
 - [11] T. Ando, J. Phys. Soc. Japan **69**, 1757 (2000).
 - [12] J.-S. Jeong and H.-W. Lee, Phys. Rev. B **80**, 075409 (2009).
 - [13] W. Izumida, K. Sato, and R. Satoito, J. Phys. Soc. Japan **78**, 074707 (2009).
 - [14] L. Chico, M. P. López-Sancho, and M. C. Muñoz, Phys. Rev. B **79**, 235423 (2009).
 - [15] F. Kuemmeth *et al.*, Nature **452**, 448 (2008).
 - [16] D. V. Bulaev, B. Trauzettel, and D. Loss, Phys. Rev. B **77**, 235301 (2008).
 - [17] T. Ando, J. Phys. Soc. Japan **74**, 777 (2005).
 - [18] J. C. Slonczewski and P. R. Weiss, Phys. Rev. **109**, 272 (1958).
 - [19] Evaluating the Δ_1 in Ref. [15], the contribution of first term $\sim \Delta_0$ in Eq. (3) was not taken into account. It does not matter if $\cos 3\theta \approx 0$; we suppose that this was the case for the actual CNT in Ref. 15.
 - [20] H. O. H. Churchill *et al.*, Phys. Rev. Lett. **102**, 166802 (2009).
 - [21] Y. G. Semenov, Phys. Rev. B **67**, 115319 (2003); Y. G. Semenov and K. W. Kim, *ibid* **75**, 195342 (2007).
 - [22] G. E. Pikus and A. N. Titkov, in *Optical Orientation*, Ed. F. Meier and B. P. Zakharchenia (Elsevier, Amsterdam, 1984), Chap. 3.
 - [23] B. F. Habenicht, S. V. Kilina, and O. V. Prezhdo, Pure Appl. Chem. **80**, 1433 (2008).

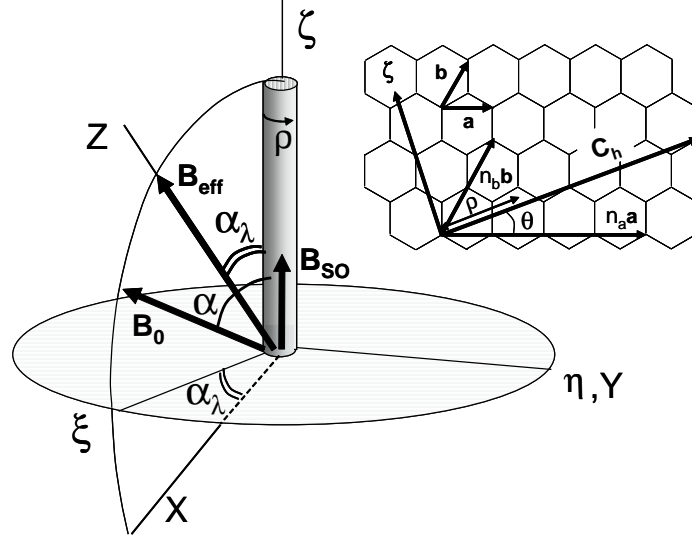


FIG. 1: Reciprocal positions of CNT and coordinate systems. Insert: the lattice structure of graphene.

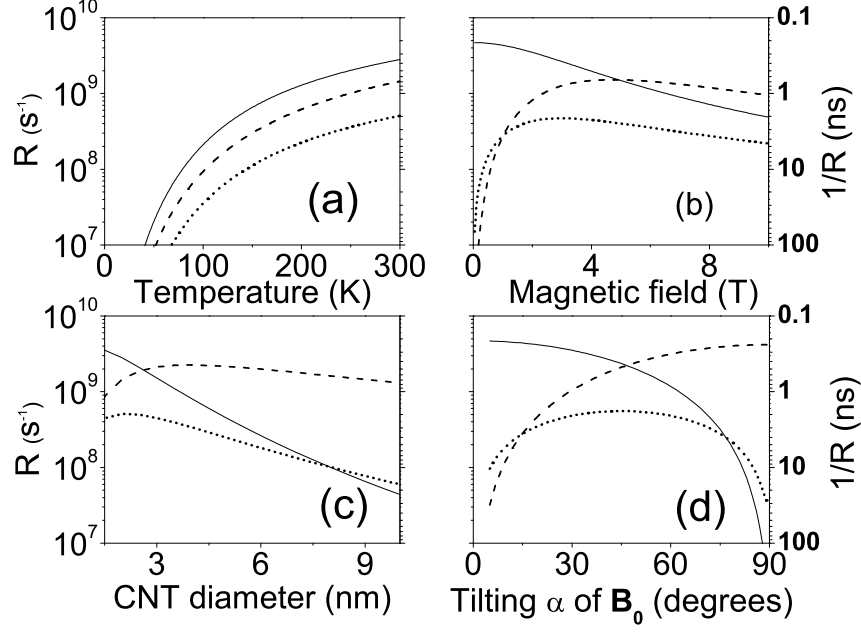


FIG. 2: R_{XX} (solid lines), R_{ZZ} (dashed lines) and R_{XZ} (dotted lines) calculated as an average over valleys and the functions of (a) temperature $[(n_a, n_b) = (15, 14), B_0 = 2 \text{ T}, \alpha = \pi/2]$, (b) magnetic field strength $[(n_a, n_b) = (15, 14), T = 300 \text{ K}, \alpha = \pi/2]$, (c) the nanotube diameter $[T = 300 \text{ K}, B_0 = 2 \text{ T}, \alpha = \pi/2, \theta = 27^\circ]$ and (d) the angle α between external magnetic field direction and CNT axis $[(n_a, n_b) = (17, 13), T = 300 \text{ K}, B_0 = 2 \text{ T}]$. For convenience the right parts of the graphs are scaled in nanoseconds as a reciprocal values.

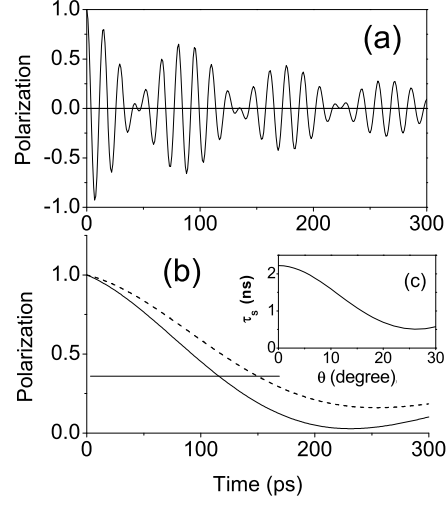


FIG. 3: (a) $(n_a, n_b) = (15, 14)$, $B_0 = 0.2$ T and $\alpha = 30^\circ$ (b) $(n_a, n_b) = (17, 13)$, $B_0 = 0.05$ T and $\alpha = 90^\circ$. Solid (dashed) lines corresponds to transversal P_ξ (longitudinal P_ζ) spin polarization. Thin horizontal line cuts the polarization curves at the level $1/e$, which indicates the relaxation times 110 ps and 150 ps for P_ξ and P_ζ . Insert (c) displays the dependence of relaxation time τ_S on chiral angle calculated with Eq. (12) under constant $d = 10$ nm, $B_0 = 2$ T and $\alpha = 90^\circ$.